IMMUNOLOGY

Red blood cell–derived nanoerythrosome for antigen delivery with enhanced cancer immunotherapy

Xiao Han[1]*, Shufang Shen[1]*, Qin Fan[1], Guojun Chen[2], Edikan Archibong[3], Gianpietro Dotti[3], Zhuang Liu[1†], Zhen Gu[2,4†], Chao Wang[1†]

Erythrocytes or red blood cells (RBCs) represent a promising cell-mediated drug delivery platform due to their inherent biocompatibility. Here, we developed an antigen delivery system based on the nanoerythrosomes derived from RBCs, inspired by the splenic antigen-presenting cell targeting capacity of senescent RBCs. Tumor antigens were loaded onto the nanoerythrosomes by fusing tumor cell membrane–associated antigens with nanoerythrosomes. This tumor antigen–loaded nanoerythrosomes (nano-Ag@erythrosome) elicited antigen responses in vivo and, in combination with the anti–programmed death ligand 1 (PD-L1) blockade, inhibited the tumor growth in B16F10 and 4T1 tumor models. We also generated a tumor model showing that "personalized nano-Ag@erythrosomes" could be achieved by fusing RBCs and surgically removed tumors, which effectively reduced tumor recurrence and metastasis after surgery.

INTRODUCTION

Immune checkpoint blockade (ICB) therapy unleashes the patient's immune system, resulting in the tumor regression of various types of cancer (*1*–*4*). However, the response rate remains low in several malignancies, and immune-related adverse events can occur after ICB therapy, indicating that this strategy requires improvements to maximize activity while reducing toxicity (*5*–*9*). The combination of ICB with other treatments has been demonstrated to improve the response rate (*10*–*13*). Among them, several clinical trials have verified that immune responses could be elicited in cancer patients by cancer vaccines (*14*–*16*), but the achievement of objective clinical responses remains challenging (*17*, *18*). Possible reasons include the immunosuppressive nature of the tumor microenvironment [for example, a high level of programmed death ligand 1 (PD-L1) expression in tumor cells]. In addition, PD-L1 expression on antigen-presenting cells (APCs) failed to induce T cell proliferation and furthermore was able to induce T regulatory cells (*19*). Therefore, the combination of anti–PD-L1 (aPDL1) with cancer vaccine could be beneficial.

In addition, the inefficient delivery of tumor antigens to professional APCs in vivo (*20*) contributes to reducing the potency of cancer vaccines. Over the past few decades, various antigen delivery systems have been reported in animal models. Micro-/nanoformulations and macroscale biomaterials as effective antigen delivery tools and/or as adjuvants for improving immune response could generate robust antitumor immune response compared with free antigen (*16*, *21*–*27*). However, many of them are synthetic materials and need chemical conjunction. The safety profile of such systems is often concerned regarding physiological interaction and metabolism for clinical practice.

Here, we report a combination of cancer vaccine based on the erythrocyte membrane and aPDL1 blockade. Because of their inherent biocompatibility, the red blood cells (RBCs) have been widely studied for drug delivery (*28*, *29*). Notably, senescent or damaged RBCs are physiologically eliminated by scavenger cells, such as macrophages and dendritic cells (DCs) within the spleen (*30*, *31*). Spleen is a critical secondary lymphoid organ in which B cells, T cells, natural killer (NK) cells, and APCs such as DCs are particularly abundant (*23*). We thus hypothesized that damaged RBC could be leveraged to deliver tumor-associated antigens (TAAs) to APCs in a critical secondary lymphoid organ. To this end, nanosized RBC–tumor membrane vesicles or nanoerythrosomes through sonication and membrane extrusion (*32*) were fused with the membrane of tumor cells to obtain nano-Ag@erythrosome (*33*). In vivo delivery of nano-Ag@erythrosome effectively reached splenic APCs and activates T cell immune responses. In mouse B16F10-Luc and 4T1 tumor models, the combination of nano-Ag@erythrosome and ICB caused tumor regression. Furthermore, "personalized vaccination" with nano-Ag@erythrosome obtained by fusing RBCs with resected tumors allowed inhibition of tumor recurrence and metastases, mimicking a clinical situation.

RESULTS

Characterization of nano-Ag@erythrosome

We engineered RBC membrane vesicles (nanoerythrosomes) by fusing ghost RBCs and tumor cell membrane with the desired ratio (Fig. 1A). As shown by the transmission electron microscopy (TEM) and dynamic light scattering (DLS) analyses, tumor membrane–fused nanoerythrosomes (nano-Ag@erythrosome) were obtained via sonication and physical extrusion (Fig. 1B and figs. S1 and S2). Nanoerythrosomes showed rapid clearance from the blood into the spleen upon systemic administration via intravenous injection, making them an effective vehicle for the targeted spleen delivery. SDS–polyacrylamide gel electrophoresis (SDS-PAGE) was performed to verify antigen load on nano-Ag@erythrosome. Compared to the tumor cell membranes or nanoerythrosomes, nano-Ag@erythrosome

[1]Institute of Functional Nano & Soft Materials (FUNSOM), Jiangsu Key Laboratory for Carbon-based Functional Materials and Devices, Soochow University, Suzhou, Jiangsu 215123, China. [2]Department of Bioengineering, University of California, Los Angeles, Los Angeles, CA 90095, USA. [3]Division of Molecular Pharmaceutics and Center for Nanotechnology in Drug Delivery, Eshelman School of Pharmacy, University of North Carolina at Chapel Hill, Chapel Hill, NC 27599, USA. [4]California NanoSystems Institute, Jonsson Comprehensive Cancer Center, University of California, Los Angeles, Los Angeles, CA 90095, USA.
*These authors contributed equally to this work.
†Corresponding author. Email: cwang@suda.edu.cn (C.W.); guzhen@ucla.edu (Z.G.); zliu@suda.edu.cn (Z.L.)

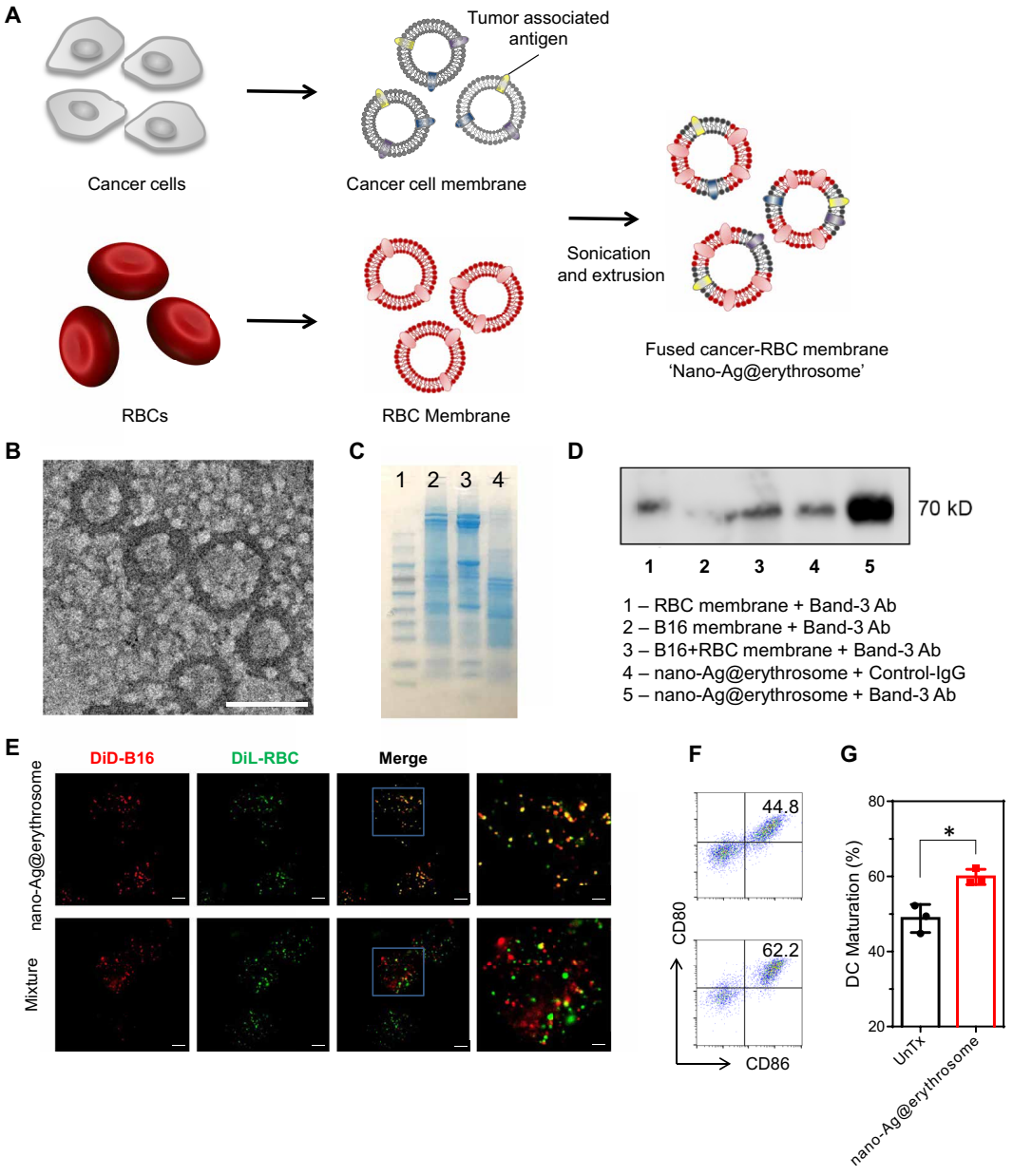

Fig. 1. Schematic and characterization of nano-Ag@erythrosomes. (**A**) Schematic of preparation of nano-Ag@erythrosomes by fusing tumor antigen–associated cell membrane into nanoerythrosomes. (**B**) Representative TEM image of nano-Ag@erythrosomes. Scale bar, 250 nm. (**C**) SDS-PAGE pattern of proteins from (1) marker, (2) nano-Ag@erythrosomes, (3) B16F10 cell membrane, and (4) RBC cell membrane. (**D**) Western blot result of gp100 on various groups after immunoprecipitation with anti–Band-3. Equal quantities of protein from each sample were subjected to SDS-PAGE and immunoblotting with gp100-specific monoclonal antibody (Ab). Western blot showed that the tumor antigen gp100 was fused into nano-Ag@erythrosomes. (**E**) Confocal laser scanning microscopy images of mouse bone marrow–derived DCs treated with nano-Ag@erythrosomes for 2 hours. A mixture of RBC and B16F10 membranes was used as control. Scale bars, 5 μm (left) and 2 μm (right). (**F**) Representative flow cytometric analysis of maturation of mouse bone marrow–derived DCs treated in vitro with nano-Ag@erythrosomes for 12 hours and (**G**) corresponding quantification results ($n = 3$). Data are means ± SEM. Statistical significance was calculated by Student's t-test. *$P < 0.05$.

contained both proteins from RBCs and tumor cell membranes (Fig. 1C). Melanoma expresses glycoprotein 100 (gp100), which is a melanoma tumor–associated antigen that can induce cytotoxic T cells (*34*). To prove the fusion of RBC membranes, immunoprecipitation was performed before Western blot analysis. Band 3 anion transport protein is a key protein present on the erythrocyte surface. After immunoprecipitation with anti–Band-3 beads, a strong gp100 signal was observed on pull-down protein of nano-Ag@erythrosome (Fig. 1D and fig. S3). Nano-Ag@erythrosomes were incubated with DCs, and confocal microscopy imaging showed effective DC uptake of nano-Ag@erythrosome. Colocalization of fluorescent signals was observed from nano-Ag@erythrosome compared with a simple mixture of nanoerythrosomes (labeled with DiD) and tumor vehicles (labeled with DiL) (Fig. 1E). In addition, the CD80 and CD86 expression of bone marrow–derived DCs was up-regulated after incubation with nano-Ag@erythrosome (Fig. 1,

F and G). Collectively, these results show that the fused nanoerythrosomes and tumor cell membrane antigen could be formed as expected.

To evaluate the effect of nano-Ag@erythrosome on in vivo targeting of APCs, we varied RBC membrane–to–tumor cell membrane (R:T) ratios based on the protein weight. We observed that the size and ζ potential of hybrid vehicles were not affected obviously by changing the R:T ratios. The fused membrane formed stable nanoparticulate vehicles of reproducible size (about 200 nm) and charge (about −10 mV) (fig. S1). Tumor cell membranes labeled with Cy5.5 before the fusion into nano-Ag@erythrosomes were intravenously administrated into mice. We found that the increase of the R:T ratio enhanced the signal of tumor antigen in the spleen, but not in the liver and other organs. In contrast, at lower R:T ratios, RBC tumor antigen signals had a propensity to accumulate in the liver (Fig. 2, A to C, and figs. S4 and S5). To better understand the function of the components, RBC and B16 membranes were labeled with DiD and DiR, respectively, before membrane fusion. Nano-Ag@erythrosomes with an R:T ratio of 20:1 were injected intravenously. While the signal of the RBC membrane in the spleen remained almost unchanged, the signal of B16 membranes of nano-Ag@erythrosomes was greatly enhanced compared with the mixture (fig. S4). Hence, we selected nano-Ag@erythrosomes with an R:T ratio of 20:1 for the further studies.

Administration of nano-Ag@erythrosomes up-regulated stimulatory and inhibitory markers on splenic DCs and macrophages

The spleen, known as the organ consisting of the highest density of APCs, plays a central role in the detection and capture of antigens and pathogens in the circulation, as well as antigen processing to stimulate naïve T cells (*23*). We have validated that nano-Ag@erythrosomes were quickly cleared from the blood into the spleen within 1 hour after intravenous administration. Antigens delivered by nano-Ag@erythrosomes colocalized with major histocompatibility complex (MHC) II^+ APCs in the spleen, as measured by immunofluorescence imaging (Fig. 2D), suggesting effective uptake of the antigen by APCs. We have further analyzed various stimulatory and inhibitory molecules expressed on the splenic macrophages and DCs after the nano-Ag@erythrosome treatment. Nano-Ag@erythrosomes were labeled with DiD before injection. According to the flow cytometry results, the expression of various stimulatory markers including CD80, CD86, CD40, and MHC II on splenic DCs and macrophages was up-regulated after mice were treated with nano-Ag@erythrosome. Compared with DCs and macrophages without nano-Ag@erythrosome uptake, cell populations that internalized nano-Ag@erythrosome expressed higher stimulatory markers. Notably, the inhibitory molecule PD-L1 expression on DCs and macrophages was also enhanced after administration of nano-Ag@erythrosome, indicating that blockade of PD-L1 on splenic APCs in combination with nano-Ag@erythrosomes could induce potential synergetic antitumor effect (Fig. 2, E and F, and fig. S6).

Notably, splenic NK cells, B cells, $CD4^+$ T cells, and $CD8^+$ T cells were also activated by nano-Ag@erythrosomes (Fig. 2, G and H). Systemic cytokines in the serum were analyzed during the treatment. We analyzed 13 kinds of cytokines in the serum. Of note, all the cytokine levels were found elevated after 24-hour Ag@erythrosome injection, but their levels were decreased after 48 hours. All these cytokines were produced by the activated T cells, B cells, NK cells, DCs, and macrophages (Fig. 2I and fig. S7). For example, type I interferons (IFNs) are mainly produced by APCs in response to antigens. DCs and macrophages also produce some proinflammatory cytokines for an efficient inflammatory environment (*35*, *36*). Besides, we also observed some cytokines released by activated T helper 1 (T_H1) cells and NK cells. Cytokines such as IFN-γ (*37*) were increased after the 24-hour nano-Ag@erythrosome injection (Fig. 2I). Together, these results suggest that the Ag@erythrosome treatment effectively activated various immune cells.

Therapeutic efficacy of nano-Ag@erythrosomes in combination with PD-L1 blockade

We have further tested the therapeutic efficacy of nano-Ag@erythrosomes in tumor-bearing C57BL/6 mice. In the B16F10-Luc tumor model, mice received three doses of nano-Ag@erythrosomes with or without aPDL1 (Fig. 3A). While tumor growth was not affected by nano-Ag@erythrosome vaccine alone (Fig. 3, B and C), the combination with aPDL1 was effective (Fig. 3, B and C). Forty-four percent of the mice treated with nano-Ag@erythrosomes and aPDL1 survived 40 days (Fig. 3D), without notable changes in body weight (Fig. 3E). In addition, the fraction of the RBC membrane in nano-Ag@erythrosome could benefit the therapeutic efficacy compared to the B16F10 membrane alone (fig. S8), which was probably due to the insufficient spleen accumulation of B16F10 membrane vesicles. The antitumor effects were corroborated by T cell responses, as evidenced by the higher percentage of tumor-infiltrating lymphocytes (TILs) (Fig. 3, F and G) that produce IFN-γ (Fig. 3, J and K). As IFN-γ can up-regulate PD-L1 expression in tumor cells (*38*), we examined the PD-L1 expression on nonhematopoietic cells ($CD45^-$ cells) and found that the tumor has a lower PD-L1 expression on $CD45^-$ cells when combined with aPDL1 therapy, indicating that the inhibition of PD-L1 mediated T cell exhaustion in the tumor microenvironment (Fig. 3, H and I). The antitumor activity of combining nano-Ag@erythrosomes and aPDL1 was conformed in a lung B16F10-Luc and 4T1-Luc metastatic tumor model (figs. S9 and S10). Collectively, these results suggested that the anticancer immune response induced by nano-Ag@erythrosomes was amplified by aPDL1 treatment.

In cancer patients, personalized cancer vaccines may be vitally important, as genetic mutations of every individual patient lead to the expression of unique tumor antigens known as neoantigens (*39*). As malignant tumors grow, unique tumor neoantigens may be expressed. In addition, tumor cells express a whole array of TAAs, which is a good source of numbers of different tumor antigens (*40*). We therefore also implemented a model to assess whether the developed approach could inhibit recurrence and metastatic spread of the tumor after resection of the primary tumor (Fig. 4A). In B16F10-Luc tumor-bearing mice cells, tumor was surgically resected at day 7. Single-cell suspension from the removed tumor was obtained, and RBCs were collected from the same tumor-bearing mice to generate an autologous nano-Ag@erythrosomes. Mice were then inculcated in the opposite flank with B16F10-Luc tumor cells (Fig. 4B), and at day 0, treated with autologous nano-Ag@erythrosomes and aPDL1. As shown in Fig. 4, C to E, nano-Ag@erythrosomes and aPDL1 treatment controlled the growth of the secondary tumor and extended survival after surgery, without notable side effects as compared to the control group (Fig. 4F).

DISCUSSION

In the current study, we reported an antigen delivery system based on the erythrocyte membrane vehicle, nanoerythrosomes extruded

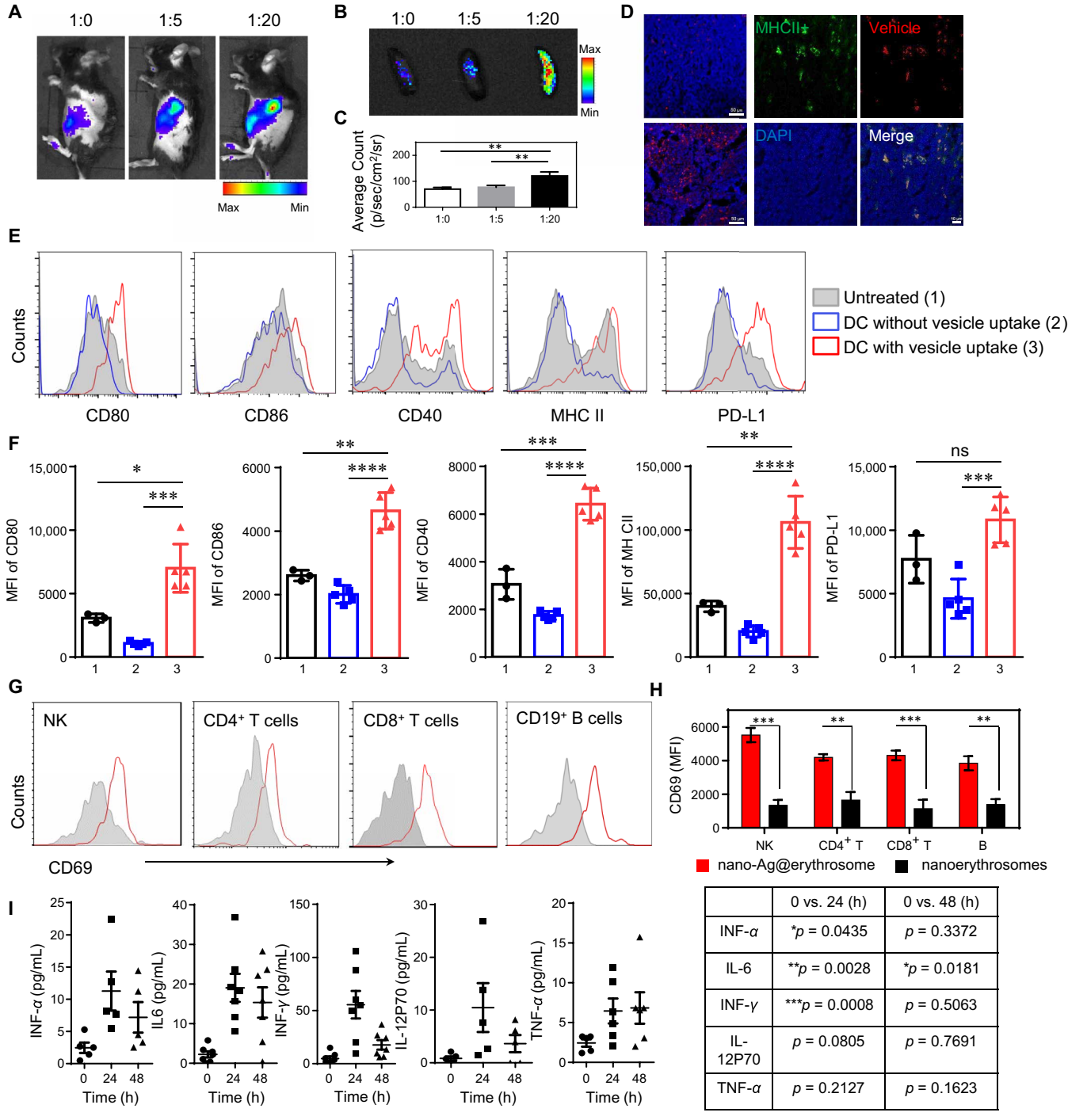

	0 vs. 24 (h)	0 vs. 48 (h)
INF-α	*p = 0.0435	p = 0.3372
IL-6	**p = 0.0028	*p = 0.0181
INF-γ	***p = 0.0008	p = 0.5063
IL-12P70	p = 0.0805	p = 0.7691
TNF-α	p = 0.2127	p = 0.1623

Fig. 2. Nano-Ag@erythrosomes target the splenic APC and induce activation of immune cells. (**A**) Fluorescence imaging of C57BL/6 mice ($n = 3$) 1 hour after intravenous injection of nano-Ag@erythrosomes at various ratios. (**B** to **D**) Ex vivo imaging of spleen 1 hour after intravenous injection of nano-Ag@erythrosomes at various ratios (B) and corresponding quantification results ($n = 3$) (C). (D) Confocal images of splenic localization of MHC II$^+$ and Cy5.5 double-positive cells in C57BL/6 mice ($n = 3$) 1 hour after intravenous injection of Cy5.5-labeled nano-Ag@erythrosomes. (Upper left: Splenocyte of mice in 1:0 group. Bottom left: Splenocyte of mice in 1:20 group.) Scale bars, 50 μm (left) and 10 μm (right). (**E**) Flow cytometric analysis of various activation markers and PD-L1 in DCs (gated on CD11c$^+$) in spleen of untreated mice and mice treated with DiD-labeled nano-Ag@erythrosome and (**F**) corresponding quantification of mean fluorescence intensity (MFI) according to (E). ns, not significant. (**G**) Activation markers measured 24 hours after intravenous injection of nano-Ag@erythrosomes in splenic immune cell subsets (red for treatment, gray for control). (**H**) Corresponding quantification of MFI according to (G) ($n = 5$). (**I**) Cytokines level in serum 24 and 48 hours after intravenous injection of nano-Ag@erythrosomes. For (F) and (H), data are means ± SD. Statistical significance was calculated by Student's *t*-test. For (C) and (I), data are means ± SEM. Statistical significance was calculated by one-way ANOVA with Tukey's post hoc test. *$P < 0.05$; **$P < 0.01$; ***$P < 0.005$; ****$P < 0.001$.

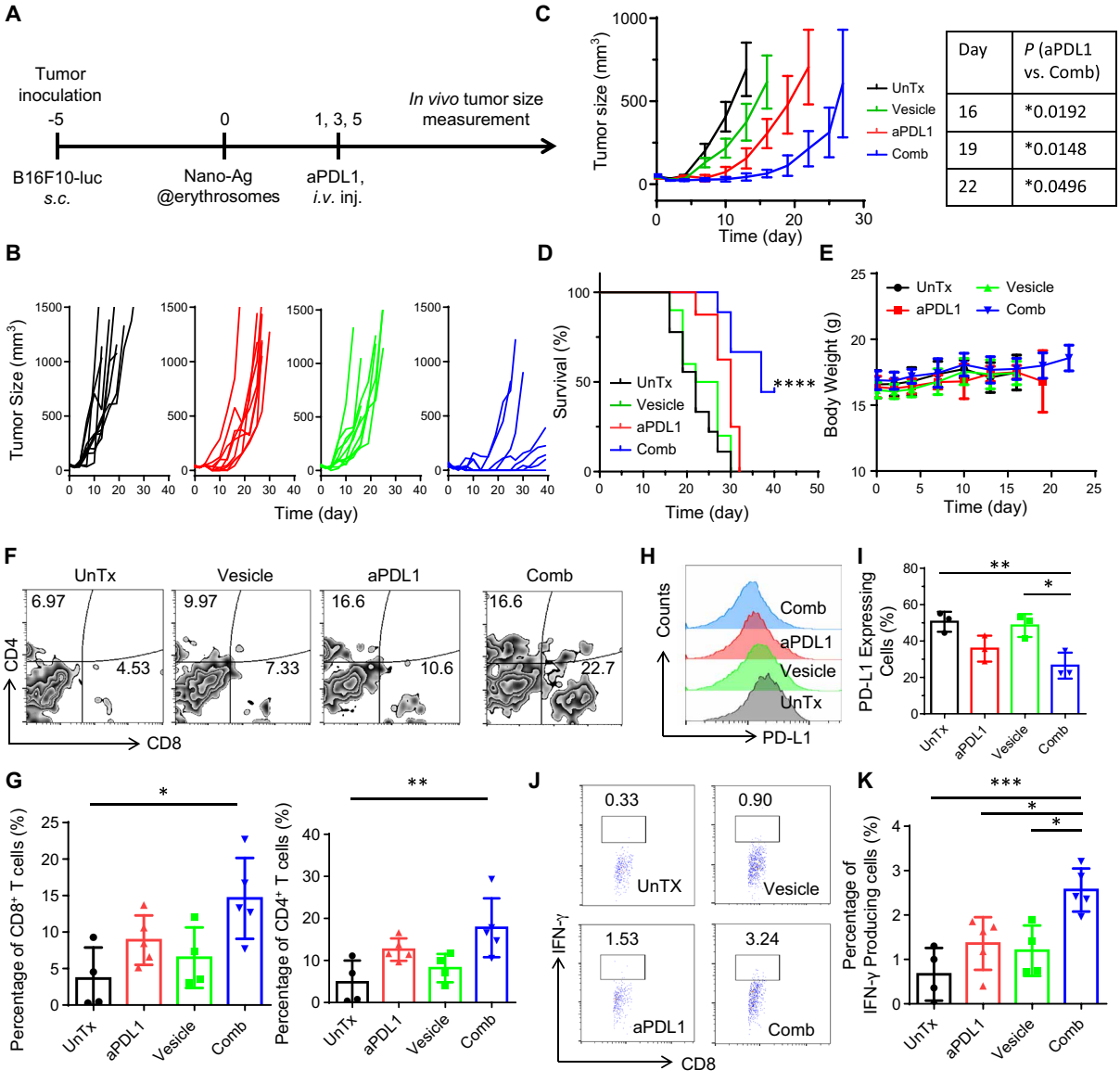

Fig. 3. Combination immunotherapy for inhibition of B16F10-Luc melanoma growth in vivo. (**A**) Schematic representation of the B16F10-Luc tumor model. s.c., subcutaneously; i.v., intravenously. (**B** and **C**) Individual (B) and average (C) tumor growth kinetics in control and treated groups ($n = 7$ to 10). Growth curves represent means ± SEM; growth curves were stopped when the first animal of the corresponding group died. Animals were euthanized when exhibiting signs of impaired health or when the volume of the tumor exceeded 1.5 cm^3. (**D**) Survival curves for the treated and control mice. (**E**) Body weight of mice after different treatments as indicated. (**F**) Representative dot plots showing the number of $CD4^+$ and $CD8^+$ T cells as a percentage of the total $CD45^+$ cell population in the tumor after different treatments as indicated and (**G**) corresponding quantification results ($n \geq 4$). (**H**) Flow cytometric analysis of PD-L1 expression in tumor (gated on $CD45^-$) after different treatments as indicated and (**I**) corresponding quantification results ($n = 3$). (**J**) Flow cytometric analysis of the percentage of intracellular IFN-γ^+ $CD8^+$ T cells in tumor after different treatments as indicated and (**K**) corresponding quantification results ($n \geq 4$). Data are means ± SEM. For (D), statistical significance was calculated by Log-rank (Mantel-Cox) test. For (I), (G) and (K), statistical significance was calculated by one-way ANOVA with Tukey's post hoc test. *$P < 0.05$; **$P < 0.01$. ***$P < 0.005$.

from RBCs, in combination with aPDL1 for combined cancer immunotherapy. Compared with other antigen delivery systems, the RBC-derived formulation could achieve competitive safety profiles. Meanwhile, tumor antigens were loaded onto the nanoerythrosomes by fusion of tumor cell membrane–associated tumor antigens with nanoerythrosomes, without any chemical reactions or chemical linkers. Therefore, it could be metabolized in the biological system without any unwanted by-products. As senescent or damaged RBCs are the targets of the macrophages and DCs of the spleen, the nanoerythrosomes have the inherent capacity to be captured by these two main APCs in our body. We have demonstrated that APCs could be targeted effectively in vivo via intravenously administered nano-Ag@erythrosomes when the R:T ratio is 20:1.

We have observed a significant activation of immune system by a single dose of nano-Ag@erythrosome administration. Unlike RBCs, the nanoscaled nano-Ag@erythrosomes may serve as adjuvants, promoting APC activation and maturation. One possible reason is that the inside-out structure of cell membrane vesicles is different from RBC (*41*). These outside-out structure vesicles might be recognized by splenic DCs for the missing self-markers including CD47. In

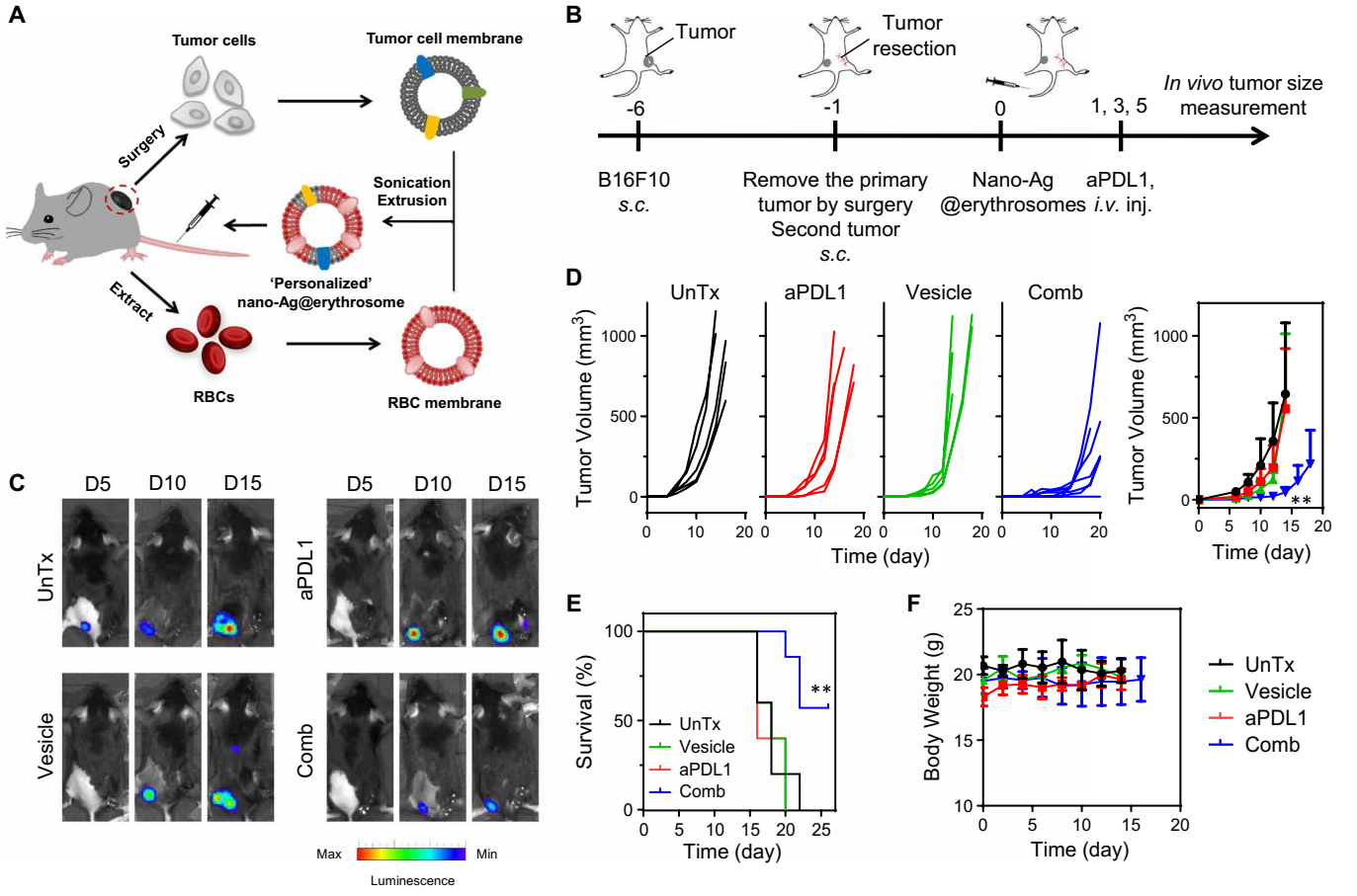

Fig. 4. Personalized nano-Ag@erythrosomes for inhibition cancer metastasis and recurrence after surgery. (**A**) Schematic of preparation of personalized nano-Ag@erythrosomes. (**B**) Schematic representation of the primary tumor resection and distant tumor model. (**C**) In vivo bioluminescence imaging of the distant B16F10-Luc tumors after different treatments as indicated. (**D**) Individual and average tumor growth kinetics in control and treated groups ($n \geq 5$). Growth curves represent means ± SEM; growth curves were stopped when the first animal of the corresponding group died. (**E**) Survival curves for the treated and control mice. (**F**) Body weight of mice after different treatments as indicated. Data are means ± SEM. For (D), statistical significance was calculated by one-way ANOVA with Tukey's post hoc test. For (E), statistical significance was calculated by Log-rank (Mantel-Cox) test. $^{**}P < 0.01$.

addition to macrophages and DCs, NK cells, B cells, and $CD4^+$ and $CD8^+$ T cells were also effectively activated, and a transient boost of serum cytokines produced by T_H1 and NK cells occurred after administration, indicating that the immune response is being activated by the antigens. However, in the mouse tumor model, the induced immune response by nano-Ag@erythrosome failed to inhibit the tumor growth. We further analyzed the stimulatory and inhibitory molecules expressed on the splenic macrophages and dendrite cells after the nano-Ag@erythrosome treatment. Both stimulatory (CD80, CD86, CD40, and MHC II) and inhibitory (PD-L1) molecules on splenic DCs and macrophages had increased expression after treatment. A higher PD-L1 expression by DCs stimulates the development of regulatory T cell populations, which results in immune tolerance. This also explains why nano-Ag@erythrosomes alone showed limited antitumor effects in Fig. 3. In addition, the immunosuppressive nature of the tumor microenvironment could also hamper the antitumor immunity. As expected, blockade of PD-L1 by antibody in combination with nano-Ag@erythrosomes induced T cell activation and synergetic antitumor effect based on our results. A strong T cell–mediated anticancer immune response and a high CD8 T cell infiltration were observed in the tumor site. Furthermore, we prepared "personalized nano-Ag@erythrosomes" by fusing surgically removed tumors and RBCs, which could lead to enhanced treatment outcome.

In summary, we developed a new approach to deliver TAAs to splenic DCs using nanoerythrosomes. This strategy could be extended to develop a personalized tumor vaccine taking into account the importance of TAAs in determining responses to either adoptive transfer of TILs or ICB therapy. Furthermore, this erythrosome-based platform technology could be integrated with other membrane fusing with specific cargos to treat different diseases. In future studies, nonmembrane neoantigens could be also delivered by our vaccine formulation by chemical modification or loaded inside the platform.

MATERIALS AND METHODS

Cell lines

The mouse melanoma cell line B16F10-Luc and the mouse mammary carcinoma cell line 4T1-Luc were obtained from the American Type Culture Collection. B16F10-Luc and 4T1-Luc cells were obtained from PerkinElmer. The culture medium for B16F10-Luc cells was Dulbecco's modified Eagle's medium (HyClone) containing 10% fetal bovine serum (Invitrogen) and penicillin and streptomycin

(100 U ml^{-1}) (Invitrogen). The culture medium for 4T1-Luc cells was RPMI 1640 medium (HyClone) containing 10% fetal bovine serum (Invitrogen) and penicillin and streptomycin (100 U ml^{-1}) (Invitrogen). Cells were tested every 3 months for potential mycoplasma. Re-authentication of cells was not performed after receipt.

Animals

C57BL/6 and Balb/c mice (6 to 10 weeks) were purchased from Changzhou Cavens Experimental Animal Co. Ltd. Mice were treated under protocols approved by the Institutional Animal Care and Use Committee.

Preparation of nano-Ag@erythrosomes

The whole blood was first collected from the orbital sinus of C57 mice and stored in phosphate-buffered saline (PBS) containing EDTA. Then, RBCs were separated from whole blood by centrifugation (2000 rpm, 5 min). The RBC membrane was obtained by a previously reported hypotonic treatment (*42*). Briefly, deionized water containing EDTA was added into the obtained RBCs, and the mixture was shaken gently for 5 min. The mixture was centrifuged at 4000 rpm for 10 min, and the supernatant was collected and further centrifuged at 14,800 rpm for 20 min at 4°C. Deionized water containing EDTA was added to the precipitation at the first step, and the solution was sonicated for 10 s, followed by centrifugation at 14,800 rpm for 20 min at 4°C. The procedure was repeated twice. The obtained RBC membrane was washed twice with deionized water containing EDTA to remove the hemoglobin.

To obtain the B16F10 membrane, the cells were suspended with homogenization medium [0.25 M sucrose, 1 mM EDTA, 20 mM Hepes-NaOH, and protease inhibitor cocktail (pH 7.4)]. The cells were sonicated using Selecta Sonopuls for 30 rounds on ice (T_{on} = 3 s, T_{off} = 7 s). The solution was centrifuged at 4000 rpm for 10 min, and the supernatant was collected and further centrifuged at 14,800 rpm for 20 min. The obtained B16F10 cell membrane was washed twice with PBS.

To obtain cell membrane from tumor tissue, B16F10 or 4T1 tumor tissues were collected and cut into pieces, followed by sonication using Selecta Sonopuls for 30 rounds on ice (T_{on} = 3 s, T_{off} = 7 s). For B16F10 tumor, the mixture was centrifuged at 6000 rpm for 10 min to remove melanin (for 4T1-Luc tumor, this step was skipped), and the supernatant was collected and further centrifuged at 14,800 rpm for 20 min.

The protein amount in the RBC and B16F10 membranes was determined using a BCA kit. The mixture of both membranes was sonicated for 15 min until the mixture solution became transparent. During this step, ice was added into the sonicator to avoid protein denaturation caused by heat. Then, the mixture was gently shaken using a dry bath incubator at 37°C for 30 min before extrusion through a 400-nm membrane.

Characterization of nano-Ag@erythrosomes

The size and surface ζ potential of the hybrid membrane vesicle were measured by DLS. TEM images were obtained using a TECNAI G2 F20 transmission electron microscope. The samples were negatively stained with sodium phosphotungstate solution.

To conduct the membrane colocalization, the RBC membrane was labeled with DiD and the B16F10 membrane was labeled with DiL before extrusion. The fused membrane vesicles, as well as the mixed individual erythrocyte and tumor membrane vesicles, were cocultured with DC 2.4 for 12 hours. Then, the cells were stained with 4′,6-diamidino-2-phenylindole (DAPI) and analyzed using a confocal microscope.

Immunoprecipitation and Western blot

The immunoprecipitation of B16F10 cell membrane, RBC membrane, membrane mixture, and the fused nano-Ag@erythrosome was conducted using a protein binding immunoprecipitation kit (abs955, Absin) according to the manufacturer's protocols. The protein amount of all the samples was determined using a BCA kit before Western blot. For each well, the protein amount was quantified to ~40 μg. All the samples were first incubated with anti–Band-3 or immunoglobulin G (IgG)–bound beads (18566-1-AP, Proteintech). The level of gp100 enriched on beads was then measured by Western blotting. Electrophoresis was conducted on 15% SDS–polyacrylamide gel and transferred onto polyvinylidene fluoride membranes (Merck Millipore, USA). Then, the samples were incubated with primary antibody of gp100 (Anti-Melanoma gp100 antibody, ab137078, Abcam), followed by horseradish peroxidase–labeled goat anti-rabbit IgG (H+L) (BA1054, BOSTER). The protein signals were detected with an enhanced chemiluminescence method using an Amersham Imager 600 imaging system (General Electric Company, USA).

Flow cytometry

Mice were intravenously injected with DiD-labeled nano-Ag@erythrosomes (RBC:B16F10 membrane protein, 20:1; B16F10 membrane protein, 10 μg). After 12 hours, mice were sacrificed and spleen was collected into single-cell suspensions. Splenocytes (2×10^6) were stained with fluorescein isothiocyanate (FITC)–CD11c, phycoerythrin (PE)–CD80, PE-CD86, PE-CD40, PE–MHC II and PE–PD-L1 for DC analysis and FITC-F4/80, peridinin chlorophyll protein (PerCP)–CD11b, PE-CD80, PE-CD86, PE-CD40, PE–MHC II, and PE–PD-L1 for macrophage analysis. The cells were analyzed using a FACSCalibur flow cytometer (BD Biosciences).

The mice were sacrificed at day 12, and tumors were collected and cut into pieces. The tumor tissues were homogenized in PBS containing 1% fetal bovine serum and filtrated through nylon gauze to obtain single-cell suspensions. The primary antibodies used for flow cytometry were purchased from BioLegend. The stained cells were analyzed with the FlowJo software package (version 10.0.7; TreeStar, USA, 2014).

In vivo distribution study

The B16 cells were first stained with DiD before obtaining the B16 membrane and fusing with the erythrocyte membrane at different ratios (1:0, 1:5, and 1:20). The fused membrane vehicles were intravenously injected into healthy C57 mice. After 1 hour, the mice were sacrificed, and the major organs were collected and imaged using an IVIS spectrum imaging system.

In vivo tumor models

The aPDL1 antibody used in vivo was purchased from Bio X Cell (clone: 10F.9G2). C57 mice were subcutaneously injected B16F10-Luc (1×10^6). Mice were weighed and randomly divided into different groups (n = 5 to 10). Seven days later, nano-Ag@erythrosomes (10 μg) and aPDL1 (2 mg/kg) were intravenously injected into mice. An IVIS Lumina imaging system (Caliper) was used to monitor the bioluminescence signal generated by cancer cells. The tumors were also measured with a digital caliper. Tumor volume was calculated according to the following formula: $width^2 \times length \times 0.5$.

In another model, B16F10-Luc cells (1×10^6) were subcutaneously injected on the right flank of C57 mice and grew for 10 days. Then, B16-luc cells (1×10^6) were subcutaneously injected on the left flank 1 day before removing the first tumor by surgery. The cell membrane was extracted according to the method described above, the protein amount of which was determined with a BCA kit. The cell membrane from the tumor and the erythrocyte membrane were fused at a ratio of 1:20. For each mouse, 10-μg proteins from the cell membrane from the tumor were used. Fused membrane vehicle as well as aPDL1 (2 mg/kg) were intravenously injected into these mice at days 1, 3, and 5 after surgery.

To conduct the metastasis model, 4T1-Luc cells (1×10^6) were first injected subcutaneously on Balb/c mice. 4T1-Luc cells (1×10^5) suspended in PBS were intravenously injected into these mice 1 day before removing the first 4T1-Luc tumor by surgery. The treatment at the same dose was repeated as the method described above.

In vivo bioluminescence and imaging

An IVIS spectrum imaging system was used to acquire the bioluminescence images at 10 min after intraperitoneal injection of D-luciferin (PerkinElmer) in PBS (15 mg ml^{-1}) into the animals (10 μl g^{-1} body weight). Exposure time was 5 min for the bioluminescence imaging.

Statistical analysis

All results are expressed as the mean ± SEM or SD as indicated. One-way analysis of variance (ANOVA), Student's *t*-test and Tukey's post hoc tests were used when more than two groups were compared. Statistical differences in survival rate were determined with the log-rank test. All statistical analyses were performed using the Prism software package (Prism 5.0; GraphPad Software, USA, 2007). The threshold for statistical significance was $P < 0.05$.

SUPPLEMENTARY MATERIALS

Supplementary material for this article is available at http://advances.sciencemag.org/cgi/content/full/5/10/eaaw6870/DC1

Fig. S1. Particle size and ζ potential of nano-Ag@erythrosomes at various ratios of RBC to B16F10 cell membrane.
Fig. S2. TEM images of RBC vesicles and B16 vesicles.
Fig. S3. Raw Western blot data according to Fig. 1D.
Fig. S4. Signal of B16 and RBC membranes in major organs.
Fig. S5. Ex vivo imaging of major organs after intravenous injection of nano-Ag@erythrosomes.
Fig. S6. Flow cytometric analysis in macrophages in spleen.
Fig. S7. Cytokine production in serum after intravenous injection of nano-Ag@erythrosomes.
Fig. S8. B16F10-Luc tumor growth curve after mice were treated with nano-Ag@erythrosomes or B16 membrane vesicle with aPDL1.
Fig. S9. In vivo therapeutic efficacy of nano-Ag@erythrosomes with aPDL1 in a B16F10-Luc lung metastasis model.
Fig. S10. In vivo therapeutic efficacy of nano-Ag@erythrosomes with aPDL1 in a 4T1-Luc lung metastasis model.

View/request a protocol for this paper from *Bio-protocol*.

REFERENCES AND NOTES

1. W. Zou, J. D. Wolchok, L. Chen, PD-L1 (B7-H1) and PD-1 pathway blockade for cancer therapy: Mechanisms, response biomarkers, and combinations. *Sci. Transl. Med.* **8**, 328rv324 (2016).
2. A. Ribas, J. D. Wolchok, Cancer immunotherapy using checkpoint blockade. *Science* **359**, 1350–1355 (2018).
3. M. F. Sanmamed, L. Chen, A paradigm shift in cancer immunotherapy: From enhancement to normalization. *Cell* **175**, 313–326 (2018).
4. J. Tang, J. X. Yu, V. M. Hubbard-Lucey, S. T. Neftelinov, J. P. Hodge, Y. Lin, The clinical trial landscape for PD1/PDL1 immune checkpoint inhibitors. *Nat. Rev. Drug Discov.* **17**, 854–855 (2018).
5. M. A. Postow, R. Sidlow, M. D. Hellmann, Immune-related adverse events associated with immune checkpoint blockade. *N. Engl. J. Med.* **378**, 158–168 (2018).
6. S. L. Topalian, J. M. Taube, R. A. Anders, D. M. Pardoll, Mechanism-driven biomarkers to guide immune checkpoint blockade in cancer therapy. *Nat. Rev. Cancer* **16**, 275–287 (2016).
7. J. J. Moslehi, J.-E. Salem, J. A. Sosman, B. Lebrun-Vignes, D. B. Johnson, Increased reporting of fatal immune checkpoint inhibitor-associated myocarditis. *Lancet* **391**, 933 (2018).
8. R. S. Riley, C. H. June, R. Langer, M. J. Mitchell, Delivery technologies for cancer immunotherapy. *Nat. Rev. Drug Discov.* **18**, 175–196 (2019).
9. C. Wang, Y. Ye, Q. Hu, A. Bellotti, Z. Gu, Tailoring biomaterials for cancer immunotherapy: Emerging trends and future outlook. *Adv. Mater.* **29**, 1606036 (2017).
10. R. Zappasodi, T. Merghoub, J. D. Wolchok, Emerging concepts for immune checkpoint blockade-based combination therapies. *Cancer Cell* **33**, 581–598 (2018).
11. S. A. Patel, A. J. Minn, Combination cancer therapy with immune checkpoint blockade: Mechanisms and strategies. *Immunity* **48**, 417–433 (2018).
12. K. D. Moynihan, C. F. Opel, G. L. Szeto, A. Tzeng, E. F. Zhu, J. M. Engreitz, R. T. Williams, K. Rakhra, M. H. Zhang, A. M. Rothschilds, S. Kumari, R. L. Kelly, B. H. Kwan, W. Abraham, K. Hu, N. K. Mehta, M. J. Kauke, H. Suh, J. R. Cochran, D. A. Lauffenburger, K. D. Wittrup, D. J. Irvine, Eradication of large established tumors in mice by combination immunotherapy that engages innate and adaptive immune responses. *Nat. Med.* **22**, 1402–1410 (2016).
13. C. Wang, J. Wang, X. Zhang, S. Yu, D. Wen, Q. Hu, Y. Ye, H. Bomba, X. Hu, Z. Liu, G. Dotti, Z. Gu, In situ formed reactive oxygen species–responsive scaffold with gemcitabine and checkpoint inhibitor for combination therapy. *Sci. Transl. Med.* **10**, eaan3682 (2018).
14. P. A. Ott, Z. Hu, D. B. Keskin, S. A. Shukla, J. Sun, D. J. Bozym, W. Zhang, A. Luoma, A. Giobbie-Hurder, L. Peter, C. Chen, O. Olive, T. A. Carter, S. Li, D. J. Lieb, T. Eisenhaure, E. Gjini, J. Stevens, W. J. Lane, I. Javeri, K. Nellaiappan, A. M. Salazar, H. Daley, M. Seaman, E. I. Buchbinder, C. H. Yoon, M. Harden, N. Lennon, S. Gabriel, S. J. Rodig, D. H. Barouch, J. C. Aster, G. Getz, K. Wucherpfennig, D. Neuberg, J. Ritz, E. S. Lander, E. F. Fritsch, N. Hacohen, C. J. Wu, An immunogenic personal neoantigen vaccine for patients with melanoma. *Nature* **547**, 217–221 (2017).
15. J. Banchereau, K. Palucka, Immunotherapy: Cancer vaccines on the move. *Nat. Rev. Clin. Oncol.* **15**, 9–10 (2018).
16. R. Kuai, L. J. Ochyl, K. S. Bahjat, A. Schwendeman, J. J. Moon, Designer vaccine nanodiscs for personalized cancer immunotherapy. *Nat. Mater.* **16**, 489–496 (2016).
17. M. A. Cheever, C. S. Higano, PROVENGE (Sipuleucel-T) in prostate cancer: The first FDA-approved therapeutic cancer vaccine. *Clin. Cancer Res.* **17**, 3520–3526 (2011).
18. E. Jäger, D. Jäger, A. Knuth, Clinical cancer vaccine trials. *Curr. Opin. Immunol.* **14**, 178–182 (2002).
19. H. Lin, S. Wei, E. M. Hurt, M. D. Green, L. Zhao, L. Vatan, W. Szeliga, R. Herbst, P. W. Harms, L. A. Fecher, P. Vats, A. M. Chinnaiyan, C. D. Lao, T. S. Lawrence, M. Wicha, J. Hamanishi, M. Mandai, I. Kryczek, W. Zou, Host expression of PD-L1 determines efficacy of PD-L1 pathway blockade–mediated tumor regression. *J. Clin. Invest.* **128**, 805–815 (2018).
20. H. Wang, D. J. Mooney, Biomaterial-assisted targeted modulation of immune cells in cancer treatment. *Nat. Mater.* **17**, 761–772 (2018).
21. A. W. Li, M. C. Sobral, S. Badrinath, Y. Choi, A. Graveline, A. G. Stafford, J. C. Weaver, M. O. Dellacherie, T.-Y. Shih, O. A. Ali, J. Kim, K. W. Wucherpfennig, D. J. Mooney, A facile approach to enhance antigen response for personalized cancer vaccination. *Nat. Mater.* **1**, 528–534 (2018).
22. A. S. Cheung, D. K. Zhang, S. T. Koshy, D. J. Mooney, Scaffolds that mimic antigen-presenting cells enable ex vivo expansion of primary T cells. *Nat. Biotechnol.* **36**, 160–169 (2018).
23. L. M. Kranz, M. Diken, H. Haas, S. Kreiter, C. Loquai, K. C. Reuter, M. Meng, D. Fritz, F. Vascotto, H. Hefesha, C. Grunwitz, M. Vormehr, Y. Hüsemann, A. Selmi, A. N. Kuhn, J. Buck, E. Derhovanessian, R. Rae, S. Attig, J. Diekmann, R. A. Jabulowsky, S. Heesch, J. Hassel, P. Langguth, S. Grabbe, C. Huber, Ö. Türeci, U. Sahin, Systemic RNA delivery to dendritic cells exploits antiviral defence for cancer immunotherapy. *Nature* **534**, 396–401 (2016).
24. C. G. Park, C. A. Hartl, D. Schmid, E. M. Carmona, H. J. Kim, M. S. Goldberg, Extended release of perioperative immunotherapy prevents tumor recurrence and eliminates metastases. *Sci. Transl. Med.* **10**, eaar1916 (2018).
25. M. Luo, H. Wang, Z. Wang, H. Cai, Z. Lu, Y. Li, M. Du, G. Huang, C. Wang, X. Chen, M. R. Porembka, J. Lea, A. E. Frankel, Y. X. Fu, Z. J. Chen, J. Gao, A STING-activating nanovaccine for cancer immunotherapy. *Nat. Nanotechnol.* **12**, 648–654 (2017).
26. Y. Xia, J. Wu, W. Wei, Y. Du, T. Wan, X. Ma, W. An, A. Guo, C. Miao, H. Yue, S. Li, X. Cao, Z. Su, G. Ma, Exploiting the pliability and lateral mobility of Pickering emulsion for enhanced vaccination. *Nat. Mater.* **17**, 187–194 (2018).
27. D. S. Wilson, S. Hirosue, M. M. Raczy, L. Bonilla-Ramirez, L. Jeanbart, R. Wang, M. Kwissa, J. F. Franetich, M. A. S. Broggi, G. Diaceri, X. Quaglia-Thermes, D. Mazier, M. A. Swartz, J. A. Hubbell, Antigens reversibly conjugated to a polymeric glyco-adjuvant induce protective humoral and cellular immunity. *Nat. Mater.* **18**, 175–185 (2019).

28. X. Han, C. Wang, Z. Liu, Red blood cells as smart delivery systems. *Bioconjug. Chem.* **29**, 852–860 (2018).
29. J. Yan, J. Yu, C. Wang, Z. Gu, Red blood cells for drug delivery. *Small Methods* **1**, 1700270 (2017).
30. R. Ing, M. Segura, N. Thawani, M. Tam, M. M. Stevenson, Interaction of mouse dendritic cells and malaria-infected erythrocytes: Uptake, maturation, and antigen presentation. *J. Immunol.* **176**, 441–450 (2006).
31. A. Banz, M. Cremel, A. Rembert, Y. Godfrin, In situ targeting of dendritic cells by antigen-loaded red blood cells: A novel approach to cancer immunotherapy. *Vaccine* **28**, 2965–2972 (2010).
32. A. Lejeune, M. Moorjani, C. Gicquaud, J. Lacroix, P. Poyet, R. Gaudreault, Nanoerythrosome, a new derivative of erythrocyte ghost: Preparation and antineoplastic potential as drug carrier for daunorubicin. *Anticancer Res* **14**, 915–919 (1994).
33. D. Dehaini, X. Wei, R. H. Fang, S. Masson, P. Angsantikul, B. T. Luk, Y. Zhang, M. Ying, Y. Jiang, A. V. Kroll, W. Gao, L. Zhang, Erythrocyte–platelet hybrid membrane coating for enhanced nanoparticle functionalization. *Adv. Mater.* **29**, 1606209 (2017).
34. L. Zhou, K. Yang, S. Dunaway, Z. Abdel-Malek, T. Andl, A. L. Kadekaro, Y. Zhang, Suppression of MAPK signaling in BRAF-activated PTEN-deficient melanoma by blocking β-catenin signaling in cancer-associated fibroblasts. *Pigment Cell Melanoma Res.* **31**, 297–307 (2018).
35. T. Luft, K. C. Pang, E. Thomas, P. Hertzog, D. N. Hart, J. Trapani, J. Cebon, Type I IFNs enhance the terminal differentiation of dendritic cells. *J. Immunol.* **161**, 1947–1953 (1998).
36. H. Jonuleit, U. Kühn, G. Müller, K. Steinbrink, L. Paragnik, E. Schmitt, J. Knop, A. H. Enk, Pro-inflammatory cytokines and prostaglandins induce maturation of potent immunostimulatory dendritic cells under fetal calf serum-free conditions. *Eur. J. Immunol.* **27**, 3135–3142 (1997).
37. D. M. Frucht, T. Fukao, C. Bogdan, H. Schindler, J. J. O'Shea, S. Koyasu, IFN-γ production by antigen-presenting cells: Mechanisms emerge. *Trends Immunol.* **22**, 556–560 (2001).
38. A. J. Minn, E. J. Wherry, Combination cancer therapies with immune checkpoint blockade: Convergence on interferon signaling. *Cell* **165**, 272–275 (2016).
39. T. N. Schumacher, R. D. Schreiber, Neoantigens in cancer immunotherapy. *Science* **348**, 69–74 (2015).
40. C. L.-L. Chiang, F. Benencia, G. Coukos, Whole tumor antigen vaccines. *Semin. Immunol.* **22**, 132–143 (2010).
41. Z. Fan, H. Zhou, P. Y. Li, J. E. Speer, H. Cheng, Structural elucidation of cell membrane-derived nanoparticles using molecular probes. *J. Mater. Chem. B* **2**, 8231–8238 (2014).
42. M. Gao, C. Liang, X. Song, Q. Chen, Q. Jin, C. Wang, Z. Liu, Erythrocyte-membrane-enveloped perfluorocarbon as nanoscale artificial red blood cells to relieve tumor hypoxia and enhance cancer radiotherapy. *Adv. Mater.* **29**, 1701429 (2017).

Acknowledgments: We acknowledge the use of Instrumentation Facility at FUNSOM and Soochow University. **Funding:** This work was supported by grants from startup supports of Soochow University and the Program for Jiangsu Specially-Appointed Professors to C.W. This work was partly supported by Collaborative Innovation Center of Suzhou Nano Science & Technology, the Priority Academic Program Development of Jiangsu Higher Education Institutions (PAPD), and the 111 Project. This work was also supported by National Natural Science Foundation of China (No. 31900988), the Natural Science Foundation of Jiangsu Province (Grant No. SBK2019040088). **Author contributions:** X.H., Z.G., and C.W. designed the project. X.H., S.S., and C.W. performed the experiments and collected the data. All authors analyzed and interpreted the data, contributed to the writing of the manuscript, discussed the results and implications, and edited the manuscript at all stages. **Competing interests:** C.W. is an inventor on a pending patent related to the technology described here, filed by the China National Intellectual Property Administration (CN201910166781.4, 6 March 2019). All authors declare no other competing interests. **Data and materials availability:** All data needed to evaluate the conclusions in the paper are present in the paper and/or the Supplementary Materials. Additional data related to this paper may be requested from the authors. Correspondence and requests for materials should be addressed to C.W. (cwang@suda.edu.cn), Z.G. (guzhen@ucla.edu), and Z.L. (zliu@suda.edu.cn).

Submitted 16 January 2019
Accepted 16 September 2019
Published 23 October 2019
10.1126/sciadv.aaw6870

Citation: X. Han, S. Shen, Q. Fan, G. Chen, E. Archibong, G. Dotti, Z. Liu, Z. Gu, C. Wang, Red blood cell–derived nanoerythrosome for antigen delivery with enhanced cancer immunotherapy. *Sci. Adv.* **5**, eaaw6870 (2019).

Red blood cell–derived nanoerythrosome for antigen delivery with enhanced cancer immunotherapy

Xiao Han, Shufang Shen, Qin Fan, Guojun Chen, Edikan Archibong, Gianpietro Dotti, Zhuang Liu, Zhen Gu and Chao Wang

Sci Adv **5** (10), eaaw6870.
DOI: 10.1126/sciadv.aaw6870